High gene flow in Atlantic vent shrimp species with multiple ridge colonizations by ecotypic lineages with contrasting symbioses

Elodie Portanier[1,2§], Pierre Methou[1,3§*], Claire Daguin-Thiébaut[2], Stéphanie Ruault[2], Anne-Sophie Le Port[2], Chong Chen[4], Marjolaine Matabos[1], Didier Jollivet[2], Florence Pradillon[1*]

[1]Univ Brest, Ifremer, BEEP, F-29280 Plouzané, France.

[2]Sorbonne Université, CNRS, UMR 7144 'AD2M', DISEEM lab, Station Biologique de Roscoff, Place Georges Teissier, Roscoff, France.

[3]Institut de Systématique, Evolution, Biodiversité (ISYEB), Muséum national d'Histoire naturelle, CNRS, SU, EPHE-PSL, UA, 57 rue Cuvier, CP51, 75005 Paris, France

[4]X-STAR, Japan Agency for Marine-Earth Science and Technology (JAMSTEC), 2-15 Natsushima-cho, Yokosuka, Kanagawa 237-0061, Japan

§Contribute equally to the article

*Corresponding authors: Pierre Methou, Pierre.Methou@ifremer.fr; Florence Pradillon: florence.pradillon@ifremer.fr

Keywords: Rimicaris shrimps, population genomics, demographic history, symbiosis, hydrothermal vents, Mid-Atlantic Ridge, Mid-Cayman Spreading Center

Abstract (239 words)

Conservation concerns regarding potential mineral extraction near deep-sea hydrothermal vents have emphasised the need for a better understanding of the contemporary connectivity of various vent-endemic species, accounting for the specifics of their life-history traits and habitat requirements. *Rimicaris* shrimps are a major component of vent communities in the Atlantic Ocean, both along the Mid-Atlantic Ridge (MAR) and at the Mid-Cayman Spreading Center (MCSC). Using ddRAD sequencing, we examined the genetic differentiation of three Atlantic *Rimicaris* species to better understand their past and present migration pathways and the possible demographic history that led to their current distribution and ecology. *Rimicaris exoculata* and *R. chacei* inhabit the MAR and exhibit widespread gene flow along the ridge with no areas of restricted connectivity. *R. hybisae* occurs at the MCSC and exhibits almost no genetic difference with its congeneric from the MAR, *R. chacei*, despite the geographic distance between them and their contrasting ecologies and morphologies. Demographic inferences support a scenario of a very recent (less than 2000 generations) separation between MCSC and MAR shrimp populations, followed by a rapid expansion in both regions, possibly triggered by symbiotic development. Analyses further suggest recent or ongoing secondary contacts involving two-way migration, which is more pronounced from the MCSC towards the MAR. All together these results suggest that *R. chacei* and *R. hybisae* represent distinct forms of the same species, which we hereby synonymise as *R. chacei*, highlighting their morphological plasticity in relation to symbiosis.

1. Introduction

Deep-sea hydrothermal vents are highly fragmented and unstable habitats hosting endemic and highly specialised species that function as a metacommunity, and where long-distance dispersal of planktonic larvae can mitigate the risk of local extinction (Mullineaux et al., 2018). At the species level, the manner in which populations are connected depends on specific life-history traits, including reproductive effort, larval development and behaviour in the water column, pelagic larval duration and settlement requirements for a given habitat (Adams et al., 2012). For vents, the availability of suitable habitats depends on geological settings that drive the distribution and dynamics of sites and habitat patches (Tunnicliffe & Fowler, 1996). Hence, in a given region, co-distributed vent species may exhibit different population connectivity networks, resulting from their specific combination of biological traits and habitat requirements. This was observed in dynamic systems of the Pacific Ocean either at the fast-spreading East Pacific Rise (EPR), where vent species exhibit different genetic structures with geographical breaks occurring at various places along the ridge (Hurtado et al., 2004; Plouviez et al., 2009), or across back-arc basins of the western Pacific (Poitrimol et al., 2022).

In the Atlantic Ocean, the slower seafloor spreading rates of the Mid-Atlantic Ridge (MAR) and the Mid Cayman Spreading Center (MCSC) result in relatively long-lived vent sites, and populations are more distantly distributed and less ephemeral than those encountered on fast spreading ridges (Beaulieu et al., 2015; Matabos et al., 2025; Van Audenhaege et al., 2024). In addition, vent habitats exhibit marked spatial heterogeneity with a strong depth gradient, as well as contrasting geochemistry (Diehl & Bach, 2020; Konn et al., 2022). This results in different vent communities along the ridge (Desbruyères et al., 2000; Plouviez et al., 2015). Connectivity networks may therefore be particularly sensitive to local (at the vent field scale) disturbances, habitat choice, and self-recruitment, as the rescue effect of larvae travelling from afar may be more easily disrupted than in systems where populations are closer from each other (Mullineaux et al., 2020). In the northern MAR, all known vent fields are currently included in exploration licences for deep seafloor mineral resources, with the exception of the

vent fields south of the Azores (Menez Gwen, Lucky Strike and Rainbow) which are included in a Portuguese Marine Natural Reserve. This makes them potentially vulnerable to future mining activities (Menini & Van Dover, 2019). There is thus an urgent need to better understand large-scale connectivity networks, accounting for species with contrasting life history traits, to be able to inform spatial management strategies.

The MAR hydrothermal vents host three main faunal assemblages. Aggregations of the alvinocaridid shrimp *Rimicaris exoculata* occupy the hottest habitats near fluid orifices (Hernández-Ávila et al., 2022; Methou et al., 2022; Segonzac et al., 1993). Patches of the gastropods *Peltospira smaragdina* and *Divia briandi* together with other vent shrimps are found at intermediate temperatures on chimney walls (Cuvelier et al., 2025; Sarrazin et al., 2022) , while extensive beds of the *Bathymodiolus* mussels co-occurring with the limpet *Lepetodrilus atlanticus*, are found in cooler habitats (Desbruyères et al., 2000; Sarrazin et al., 2020). Like in dynamic systems such as the EPR, the dominant MAR species display various connectivity patterns. *Bathymodiolus* mussels as well as the gastropods *L. atlanticus* and *P. smaragdina* all exhibit marked genetic structuration along the MAR, with a common region of reduced exchange between 26°N and 36°N (Breusing et al., 2016, 2017; Faure et al., 2009; O'Mullan et al., 2001; Portanier et al. in press). In contrast, species such as the gastropod *Divia briandi* (Yahagi et al., 2019), shrimp *R. exoculata* (Teixeira et al., 2011, 2012) and their commensal dirivultid copepods *Stygiopontius pectinatus* (Gollner et al., 2016) show no genetic structuring across their known geographical distribution.

Demographic histories of species with putative expansion or contraction also influence the present-day spatial patterns of genetic variation. This can promote geographic isolation and genetic barriers when secondary contacts then occur, but also habitat sharing, which can lead to species competition or maladaptation, allowing long-term evolutionary changes, such as speciation or niche partitioning, to occur. Along the MAR, two mussels species, *Bathymodiolus azoricus* and *B. puteoserpentis* display a parapatric distribution along a depth gradient with the presence of a hybrid zone at Broken Spur (29°N) (Breusing et al., 2017; O'Mullan et al., 2001; van der Heijden et al., 2012). Genetic admixture has also been observed in the same region between genetically differentiated populations of the gastropod *P.*

89 *smaragdina* (Portanier et al., in press), which also unfrequently shares its habitat with another closely-
90 related but chemosymbiotic species *P. gargantua*. This latter situation can likely be explained by
91 specific environmental filters or niche partitioning in certain locations (Chen et al., 2025; Sarrazin et
92 al., 2022).

93 Alvinocaridid shrimps inhabit deep-water hydrothermal vents and cold seeps around the world, and are
94 generally recognized as good dispersers with high connectivity (Methou, Ogawa, et al., 2024; Thaler et
95 al., 2014; Yahagi et al., 2015; Y. Zhou et al., 2022), although exceptions of restricted regional-scale
96 structures have been reported in *Rimicaris* species from the Mariana Arc (Methou et al., 2025). In the
97 Atlantic, two species stand out due to their highly modified head morphology at the adult stage, where
98 the enlarged cephalothoracic cavity houses a diverse chemosynthetic microbial community involved in
99 the shrimp nutrition: *R. exoculata* along the MAR and *R. hybisae* at MCSC vents, that both form high
100 density assemblages around vent chimneys (Cambon-Bonavita et al., 2021; Nye et al., 2013; Ponsard
101 et al., 2013; Zbinden & Cambon-Bonavita, 2020). Another species: *R. chacei*, which has a much less
102 developed symbiosis and much smaller cephalothoracic cavity, lives sympatrically with *R. exoculata*
103 but occupies a distinct ecological niche (Methou et al., 2020, 2022). Based on mitochondrial markers,
104 *R. chacei* appears to be genetically very similar to the MCSC species *R. hybisae* (Methou, Guéganton,
105 et al., 2024; Teixeira et al., 2013; Vereshchaka et al., 2015). However, these two species have been
106 named and treated as separate species due to their distinct morphology and ecology (Nye et al., 2012;
107 Streit et al., 2015). Although *R. chacei* has similar microbial communities to *R. exoculata* and *R.*
108 *hybisae*, the anatomical changes it acquires during metamorphosis to host its symbionts are less
109 pronounced. This has been attributed to differences in how juveniles acquire their symbionts
110 immediately after settlement (Guéganton et al., 2024; Methou, Guéganton, et al., 2024).

111 The genetic closeness between *R. chacei* and *R. hybisae* could be indicative of past or present-
112 day connections between the MAR and the MCSC, despite them being almost 4000 km apart. Similarly,
113 the genetic structure of *R. exoculata* using both mitochondrial and microsatellite data indicates that
114 shrimp metapopulations are well connected over distances of thousands of kilometres between vent
115 fields of different depths (Teixeira et al., 2011, 2012). However, the use of a limited number of genetic

markers in existing studies may not reveal fine-scale genetic structure of the different *Rimicaris* species in the Atlantic. Consequently, it remains unclear whether *R. chacei* from MAR and *R. hybisae* from MCSC represent two geographic species that underwent recent allopatric speciation in their respective regions or whether they are a single species with two distinct morphological ecotypes that still exchange migrants across the Caribbean-Atlantic region. Although existing genetic evidence argues against the 'two species' hypothesis, incomplete lineage sorting and low mutation rates in markers used for phylogenetic approaches, can both result in failure to separate semi-isolated species falling in the grey zone of speciation (Roux et al., 2016).

Here, we propose to use genome-wide scans of genetic differentiation in the three Atlantic *Rimicaris* species to better understand past and contemporary migration pathways, and the possible demographic history that led to their current distribution and ecology. These new datasets will help refine the connectivity networks of *Rimicaris* shrimps and identify areas with weaker connections, if any, thus providing key information for mitigating the impact of potential extractive activities near MAR deep-sea vents. The datasets will also be used to determine whether *R. chacei* and *R. hybisae* belong to a single genetic unit with widespread distribution that exhibits ecological plasticity in response to trophic competition. As such, the study will provide insights into how niche partitioning, symbiont acquisition and migration may interact to inform hypotheses regarding the adaptive mechanisms of Atlantic *Rimicaris* shrimps.

2. Materials and Methods

2.1. Sample collection and DNA extraction

Shrimp samples were collected from eight hydrothermal vent fields on the northern MAR and the MCSC in the Caribbean Sea (see: Figure 1A and Table 1) during nine scientific cruises (Supplementary Tables S1) for *Rimicaris exoculata* (5 localities), *R. chacei* (4 localities) and *R. hybisae* (the 2 known MCSC localities) using either the HOVs *Nautile* and *Shinkai 6500*, or the ROVs *Victor 6000* and *Isis*. After their recovery on board, specimens were either preserved in 96% ethanol or individually frozen

142 at –80°C. DNA was extracted from two to three pleopods of each individual, using 96-wells extraction
143 columns (Nucleospin 96 Tissue, Macherey–Nagel) with negative extraction controls present
144 throughout. The pleopods were digested for 2 hours at 56 °C with 30 µL of Proteinase K (20 mg/mL)
145 under 350 rpm shaking. Lysates were then incubated 20 minutes at ambient temperature with 20 µL of
146 RNAse A (20 mg/mL) and transferred into Nucleospin purification columns and centrifuged at 5600
147 rpm following manufacturer's instructions. DNA was then eluted in 100 µL of BE buffer and stored in
148 96-wells plates at − 20 °C. The quality of DNA samples was checked using electrophoresis on a 0.8%
149 agarose TBE gel stained with ethidium bromide and the quantity was determined using a Qubit
150 fluorimeter (ThermoFisher Scientific).

151 *2.2. ddRAD-seq library preparation and sequencing*

152 Individual ddRAD libraries were prepared according to the protocol of (Brelsford et al., 2016), as
153 modified by (Daguin Thiebaut et al., 2021). Approximately 100 ng of DNA was digested for each
154 individual using high-fidelity *SbfI* and *MseI* restriction enzymes (New-England BioLabs). The *SbfI*
155 enzyme was chosen due to its low cutting frequency in genomic DNA, given the very large size of the
156 shrimp's duplicated genomes (>8 Gb). Ligation with adapters, purification, amplification and pooling
157 were then carried out in our laboratory (see: Daguin-Thiébaut et al. 2021 for details). A 1.5% DF marker
158 K agarose gel cassette was used to select fragments between 300 and 800 pb in a Pippin Prep
159 (SageScience), and the quality of ddRAD libraries was checked on a High Sensitivity DNA Chip using
160 a Bioanalyzer (Agilent™). The pooled libraries were then paired-end sequenced (150 bp) in two steps.
161 First, a subset of 6 individual libraries were pooled and sequenced on a NovaSeq 6000 Illumina
162 sequencer to check the library quality (n = 6 individuals, Genoscope, Centre National de Séquençage,
163 Evry, France). Then 329 individuals were sequenced in 150 paired-end reads on a Novaseq X Illumina
164 sequencer (Novogene, Cambridge, UK). For *R. chacei* and *R. hybisae*, ten samples were included as
165 triplicates in pooled libraries to enable estimation of the genotyping error rate. For *R. exoculata*, eight
166 individuals were triplicated. Each plate comprised several negative controls to ensure the absence of
167 contamination by foreign DNA.

168 *2.3. De novo assembly, SNP calling and filtering*

169 The *FastQC* v.0.11.9 software (Andrews, 2010) was used to assess the quality of the reads and the
170 *process_radtags* module of *Stacks* v.2.52 (Catchen et al., 2011; Rochette et al., 2019) was run to
171 demultiplex the individual files. Options *-c*, *-q* and *-r* were activated. These options (1) remove any read
172 with an uncalled base, (2) discard reads with low quality scores and (3) rescue barcodes and RAD-Tags.
173 The removal of adapter sequences with up to 2 mismatches was also performed with this program. As
174 there is no reference genome available for *Rimicaris* species, two *de novo* assemblies were performed:
175 one for *R. exoculata* and one for *R. chacei / R. hybisae*. Indeed, given the close genetic relationship
176 between *R. chacei* and *R. hybisae* (Methou, Guéganton, et al., 2024; Teixeira et al., 2013; Vereshchaka
177 et al., 2015) and in order to test their joint demographic history, they were processed together. The *r0.80*
178 optimisation procedure detailed in Paris et al. (2017) and (Rochette & Catchen, 2017) (see
179 Supplementary material for details) was applied to determine optimal *Stacks -M* and *-n* parameters
180 values. The selected values were *-M* = *-n* = 4 and - *M* = *-n* = 6 for *R. exoculata* and *R. chacei / R.*
181 *hybisae*, respectively (see Supplementary Figures S1 and S2). All the modules of the *Stacks* pipeline
182 were then run sequentially on the entire dataset (i.e., including all sequenced individuals). However, the
183 *cstacks* module was not run. Instead, *sstacks* with the *--catalog* option was used to agglomerate all
184 individuals on the loci catalogue obtained from the sub-sample of individuals (24 for R. exoculata and
185 40 for *R. chacei/R. hybisae*) used for parameter optimisation. For both assemblies, running the
186 *populations* module with *-r* = 0.80 was a good compromise between the number of retrieved SNPs and
187 missing data and thus retained. The maximum observed heterozygosity *(--max-obs-het*) to avoid paralog
188 assembly and the minimum alternative allele count (*--min-mac*) required to keep a SNP at a locus were
189 set to 0.80 and 10, respectively.

190 The following filtering steps were performed on the VCF file of genotypes obtained with *Stacks*
191 v.2.52 using *VCFtools* (v.0.1.16) (Danecek et al., 2011) and *R* v.4.1.0 (R Core Team 2021) to eliminate
192 SNPs linked to potential unfiltered paralogues, SNPs with too low coverage, SNPs erroneously
193 genotyped between triplicated samples and SNPs and individuals with more than 10% of missing data
194 (see Supplementary Material for details). Only the first SNP of each locus was retained for subsequent

195 analyses to avoid linkage disequilibrium over short distance between SNPs of the same radtag. Outlier
196 SNPs were filtered out using the *R* package *pcadapt* v. 4.3.3 (Luu et al., 2017; Privé et al., 2020),
197 keeping the first two principal components of the analysis for each assembly (details in Supplementary
198 material and Figures S3 and S4). All SNPs showing *p-values* < 0.05 after adjustment using *q-values*
199 (Benjamini & Hochberg, 1995) were removed. The final filtered VCFs, which included 2020
200 independent SNPs for *R. chacei/R. hybisae* (mean coverage 69.89X) and 1258 independent SNPs for
201 *R. exoculata* (mean coverage 69.32X), were produced using VCFtools individuals and SNPs white-
202 lists. All Stacks assemblies were run on the bioinformatic cluster of the ABIMS platform hosted at the
203 Station Biologique de Roscoff.

204 *2.4. Population genetics analyses*

205 To investigate the genetic structure of either *R. exoculata* or *R.chacei / R. hybisae* populations,
206 we first performed a Principal Component Analysis (PCA) and a Discriminant Analysis of Principal
207 Components (DAPC) for both assemblies using the *R* package *adegenet* v.2.1.3 (Jombart, 2008;
208 Jombart & Ahmed, 2011). The DAPC enables the identification of the optimal number of genetic
209 clusters (K) using a K-means algorithm (*find.clusters*) and the assignment of individuals to clusters
210 (*dapc*). The function *find.clusters* was run for K ranging from 1 to 10, with 1000 iterations and 100
211 different starting points. The optimal number of clusters was identified as the one that minimised the
212 BIC values. A cross-validation procedure was then used to identify the optimal number of principal
213 components to retain to perform the DAPC. Coancestry analyses were performed using the maximum
214 likelihood approach implemented in ADMIXTURE v.1.3 (Alexander & Lange, 2011; H. Zhou et al.,
215 2011) for which datasets were formatted using PLINK v.1.9 (Chang et al., 2015; Purcell et al., 2007).
216 ADMIXTURE was run 10 times, for K values ranging from 1 to 10, with the default parameters
217 (admixture allowed). Tenfold cross-validation (CV) was applied to identify the number of clusters that
218 minimised the average CV error value. Independent runs were then combined for the optimal K value
219 using CLUMPP (Jakobsson & Rosenberg, 2007) as implemented in CLUMPAK (Kopelman et al.,
220 2015). Finally, the *StAMPP R* package (Pembleton et al., 2013) was used to calculate pairwise fixation
221 indices (F_{st}) as estimated with theta proposed by (Weir & Cockerham, 1984). Fst_s were tested against

222 zero by resampling loci (n = 1000 bootstraps) to obtain confidence intervals. Genetic diversity indices
223 (observed and expected heterozygosities, nucleotide diversity π) and heterozygote deviations from
224 Hardy-Weinberg equilibrium (F_{is}) were calculated with the *populations* module of *Stacks* using all sites
225 from all ddRAD tags of the final dataset. The direction and strength of migrations between *R.chacei/R.*
226 *hybisae* populations were investigated using networks produced by DivMigrate (Sundqvist et al., 2016),
227 with both the statistics *Gst* and Jost's *D* calculated between pairs of populations under the null
228 hypothesis of an N-islands model without demographic changes. The divMigrate-online pipeline
229 (https://popgen.shinyapps.io/divMigrate-online/) was used for the analyses, with a Genepop file of
230 2,220 SNPs used as input. In the migration network, the number of migrants (*Nm*) was recalibrated
231 between 0 and 1; 0 indicating no migrants per generation and 1 indicating a minimum of one migrant
232 per generation exchanged from population A to population B. Migration asymmetry was then tested by
233 resampling genotypes between pairs of populations with 1000 bootstraps.

234 *2.5. Demographic history*

235 We used the DILS software (Fraïsse et al., 2021) to make demographic inferences taking into
236 account linked selection and heterogeneous migration across the genome. This was done on data from
237 the two geographic populations of *R. chacei* (sampled along the MAR) and *R. hybisae* (sampled along
238 the MCSC). The software employs an Approximate Bayesian Computation (ABC) framework to
239 compare observed statistics, such as the number of bi-allelic sites shared (Ss) and fixed (Sf) between
240 populations, the number of bi-allelic polymorphic sites within each species (Sx_A, Sx_B), nucleotide
241 diversities (π or θ), Tajima's D, F_{ST}, D_{xy} and Pearson's cross-correlations, and additional summary
242 statistics from the joint site-frequency spectrum (jSFS), and then compares these with statistics
243 simulated by isolation-population models, with and without migration (28 models). The software first
244 identifies the best demographic model (from 4 main models: strict isolation (SI), ancient migration
245 (AM), isolation-with-migration (IM) and secondary contact (SC)) and then identifies the best genomic
246 model to test whether migration (2m) and effective size (2N) are heterogeneous along the genome.
247 Finally, when necessary, it identifies the loci associated with barriers to gene flow. DILS also provides
248 a goodness-of-fit statistic for all statistics used in the ABC analysis, determining how well the selected

249 demographic model fits the genomic dataset. To run the two-population analysis, we used the DILS
250 Snakemake pipeline (with Snakefile_2pop) on the ABIMS cluster. This requires the use of Python, R
251 and PyPy, as specified in the DILS_2pop bash file together with a YAML file containing all the
252 information on the biological parameters (e.g. species names, filtering preferences, mutation and
253 recombination rates, prior distributions of population sizes, population splitting times and migration
254 rates), and a cluster_2pop.json file with all the information on the module runs (e.g. allocated memory,
255 run time). Before running DILS, the sequence data were filtered according to the maximum tolerated
256 N, the minimum sequence length (L_{min}) and the minimum number of individuals to be sampled at
257 random from the sequence data for each investigated locus (N_{min}). Statistics were then estimated from
258 randomly selected subsamples of 1,000 loci with 1,000 replicates. Depending on the selected best
259 population model, the estimated population parameters are as follows: Time since populations separated
260 (Tsplit, all models); time since migration stopped (T_{AM}, AM only); time since secondary contact and
261 migration (T_{SC}, SC only); population sizes of the ancestral population (N_A) and sister populations (N_1
262 and N_2); whether these populations are constant, expanding or contracting ($N_{founder1}$ and $N_{founder2}$); and
263 finally, the directional migration rates M_{12} and M_{21} estimated in the forward sense.

264

265 # 3. Results

266 ## *3.1. Population genetic structure of* Rimicaris exoculata *along the northern MAR*

267 No spatial genetic structure was detectable on the PCA for *Rimicaris exoculata* (Figure 2), but
268 2 individuals had outlier positions on the two first PCA axes (7.3% of the explained variance) (Figure
269 2A). Individuals from all vent fields overlapped with and without these outliers (Figure 2B). The DAPC
270 procedure accordingly supported K = 1 as the optimal number of clusters (see: Supplementary Figure
271 S5). The ADMIXTURE analysis also supported the hypothesis that *R. exoculata* populations form a
272 single panmictic genetic group (see: Supplementary Figure S6 for the minimal average CV error value,
273 and S7 for membership proportions from K = 2 to K = 5). At the population level, genetic diversity
274 indices were similar across all sampled populations (see: Supplementary Table S2), and pairwise Fst

275 values were in the order of 10^{-3} and did not significantly differ from zero, except for the pair Snake
276 Pit/TAG, despite them being the closest geographically (Table 2).

277 *3.2 Population genetic structure of the* Rimicaris chacei / R. hybisae *complex*

278 Analysing the genetic structure of *R. chacei / R. hybisae* using PCA revealed a slight separation
279 of individuals sampled along the MCSC (*R. hybisae*) and individuals sampled along the MAR (*R.*
280 *chacei*) on the second axis, with some overlap. However, the first two principal components only
281 explained a small proportion of genetic variance (2.42%; see Figure 3A). In the DAPC procedure, the
282 BIC was minimised for K = 1, although K = 2 received some support (see: Supplementary Figure S5).
283 Running the DAPC with K=2 on the *R. chacei/R. hybisae* genetic dataset using one discriminant
284 function and 20 PC axes (cross-validation procedure) enabled about 24% of the genetic variance to be
285 extracted, separating individuals into two groups: one comprising *R. chacei* individuals from all MAR
286 vent sites and, the other containing *R. hybisae* individuals sampled in the Mid Cayman Spreading Centre
287 (Figure 3B). Individual posterior membership probabilities in their respective clusters were all greater
288 than 0.99, suggesting a weak but reliable population differentiation.

289 Given the DAPC results with K = 2, we examined the ancestry coefficients in the context of
290 two genetic clusters even though the K = 1 solution was preferred. Overall, *R. hybisae* individuals
291 sampled at the MCSC form one group with ancestry memberships ranging from 60 to 100% for the first
292 genetic cluster. Individuals of *R. chacei* sampled along the MAR belong to a second group with ancestry
293 membership proportions ranging from 50 to 100% for the other genetic cluster. Several individuals had
294 intermediate membership proportions, but allele frequency differences between the two genetic
295 backgrounds were weak (very few outliers: only 10 above Fst=0.25) suggesting whetevthat these
296 admixed individuals were not true hybrids (Figure 3C). Interestingly, one *R. hybisae* individual (Von
297 Damm of MCSC) and three *R. chacei* individuals (TAG and Lucky Strike of MAR) were better assigned
298 to the genetic cluster dominating the other geographic locality. More admixed individuals with the
299 highest membership proportions for the alternative genetic cluster seemed to occur along the MAR than
300 along the MCSC. Indeed, the proportion of non-admixed individuals was 0.70 for the MCSC shrimps
301 and only 0.42 for the MAR shrimps.

302 Pairwise Fst values involving pairs between MCSC and MAR vent fields were around 0.02 and
303 significantly different from zero, as also evidenced by the confidence intervals not including zero (Table
304 2). Genetic differentiation was, on the opposite, negligible and, at least one order of magnitude lower
305 between either the MCSC sites or between the MAR sites. The divMigrate analysis estimated using the
306 Gst statistic found a maximum gene flow between TAG and Snake Pit, indicating a strong connection
307 between these two sites (Figure 4A). Using this statistic, a substantial gene flow with no asymmetry
308 was also observed between the MCSC and MAR sites albeit less important than the one within each
309 geographical region. However, the number of migrants estimated by Jost's *D* suggested a much greater
310 role for the MCSC Beebe site in supplying some of the MAR sites (Broken Spur and Lucky Strike) with
311 migrants, indicating significant asymmetry in migration (Figure 4B). Examining more carefully allele
312 frequency differences across 2020 loci revealed only one nearly fixed SNP between the *hybisae* and
313 *chacei* populations and just 17 outlier SNPs with a frequency difference ranging from 0.25 to 0.5.

314 *3.3. Demographic inferences for* R. chacei *and* R. hybisae

315 As population genetics analyses revealed some genetic differentiation between the MAR *R.*
316 *chacei* and MSCS *R. hybisae* shrimp populations, we investigated potential demographic scenarios
317 connecting the two geographical groups using isolation-with-migration models (Figure 5). DILS results
318 were found to be highly sensitive to the filtering conditions of the sequence dataset due to a trade-off
319 between L_{min} and max_tolerated_N because of the very small observed divergence between the two
320 taxa. The highest number of significant goodness-of-fit values for each population parameter of the best
321 demographic model were found with a max_tolerated_N = 0.05 (no more than two gaps per locus in
322 the sequence alignment) and Lmin = 140, resulting in 5,656 loci being examined in total. Decreasing N
323 to zero greatly limited the number of loci used, whereas increasing it biases the estimation of genetic
324 statistics (see Supplementary Table S3 for the number of loci retained and the p-values of goodness-of-
325 fit for statistics estimated from different filtering attempts to select the best model). Due to the small
326 number of loci used (N = 5,656), the number of sampled alleles per population and per locus was
327 restricted to 20 in order to create 20 × 20 allele jSFS matrices that minimised the number of empty
328 cases. In parallel, we increased the number of alleles used to build a 70 x 70 matrix to better estimate

329 observed diversity statistics, which were subsequently used as an input in the ABC process.
330 Consequently, for each filtering condition, we performed two DILS runs: one with jSFS and 20 alleles
331 per population and locus, and one without jSFS and with 70 alleles per population and locus. This was
332 done to check whether they produced similar genetic statistics and selected the same population model.
333 The best population model selected for the analysis of the two *R. chacei* and *R. hybisae* populations was
334 the SC_1m_2N (p-value migration vs isolation = 0.58, p-value SC vs IM = 0.63, p-value M_homo vs
335 M_hetero = 0.64 and p-value N_hetero vs N_homo = 0.56: best model in bold) with a good congruence
336 of statistics and goodness-of-fit of these statistics (Gof2) between the two DILS runs (with and without
337 jSFS) (Table S4).

338 Statistics obtained from DILS on the whole filtered SNP data such as the number of fixed sites
339 (*Sf*), the number of shared polymorphic sites (*Ss*) and, the number of species-specific polymorphic sites
340 (*Sx_chacei, Sx_hybisae*) clearly supported the very close relationship of the two taxa (*R. chacei* and *R.*
341 *hybisae*) with almost the same genetic diversity signatures and a very low divergence (Figure 5A). For
342 both runs, the observed statistics also indicated that the two ecotype populations (*R. chacei* vs. *R.*
343 *hybisae*) were close to panmixia, showing no genetic divergence (Da= 0.00003), much less population
344 differentiation (Fst= 0.0039) than previously estimated and nearly identical low levels of genetic
345 diversities (θ_{N1}=0.0027, θ_{N2}=0.0026), consistent with neutral evolution (Tajima's D= -0.61 (N1) and -
346 0.56 (N2) (Figure 5B & C). However, it is worth noting that, unlike divergence estimates, the *Fst*
347 distribution contains several outlier loci (Figure 5 C). Results first indicated that the two ecotype
348 populations emerged from a very small ancestral population (0.018 million) and then increased rapidly
349 in size (N_1=3.7 million and N_2=4.5 million), with the *R. hybisae* population initially being nearly twice
350 the size of the *R. chacei* population (Figure 5D). Since the population split, the *R. chacei* population has
351 steadily grown, while the *R. hybisae* population began contracting around 750 generations ago. The
352 ecotype populations diverged very recently (T_{split} around 2,100 generations ago) and they reunited
353 almost instantly (T_{sc} = 2,000 generations ago), suggesting that the allelic lineage sorting between the
354 two ecotypes never truly began (Figure 5D). Migration rates between the two sister populations are high
355 in both directions, but are slightly greater from *R. hybisae* to *R. chacei* (M_{12} =21 vs M_{21} =32 migrants

356 per generation). As expected, given the lack of divergence, migration is homogeneous across the
357 genome, with no barrier loci; however linked selection appears to be quite localised (β distribution of
358 *Ne*: α=0.6, β=3.7 suggesting that the low recombination rate is restricted to a few linked loci) across
359 the genome of the two species. The second-best model, selected by DILS with slightly fewer loci (N =
360 5,237), was AM_1m_2N. The population parameter means were almost identical to those of the first
361 model for N_A, N_1, N_2, T_{split}, M_{12}, M_{21}, and *Shape_N_α* and *Shape_N_β*, but T_{dem} and T_{AM} (time at which
362 migration ceased) coincided with T_{split}. This indicates a very recent period of strict isolation, followed
363 by population expansion, during which there was insufficient time for sorting alleles.

364

365 # 4. Discussion

366 *4.1. Panmictic vent shrimp populations along the MAR*

367 Genome-wide approaches employed here failed to reveal any genetic structure among the
368 populations of *Rimicaris exoculata* or *R. chacei*, which are distributed over distances of 3,000 km and
369 2,000 km, respectively, along the Mid-Atlantic Ridge. Our results therefore confirm the findings of
370 previous studies that used both mitochondrial COI gene and nuclear microsatellite markers (Teixeira et
371 al., 2011, 2012, 2013), suggesting that populations of the two shrimp species are capable of exchanging
372 larvae over long distances along the MAR. With the exception of a few outlier individuals (which may
373 be due to either DNA contamination or the presence of immigrants from elsewhere), our genomic
374 analysis, which was based on 1,258 (*R. exoculata*) and 2,220 (*R. chacei*) independent SNPs clearly
375 showed complete mixing of individuals, regardless of their geographic origin. Consequently, the
376 complete lack of genetic structure for both species along the Mid-Atlantic Ridge can only be explained
377 by highly efficient migration over the ridge axis.

378 Unfortunately, the path taken by dispersing larval stages remains enigmatic, as the only
379 evidence of their life outside the vent habitat is the photosynthetic signature of their tissue just after
380 settlement (Pond et al., 2000). Their planktonic zoea larvae exhibit morphological characteristics
381 indicative of an elongated larval phase (Hernández-Ávila et al., 2015) during which they develop in

water masses, feeding on photosynthetic material originating from the surface production in order to accumulate lipid reserves (Methou et al., 2020; Pond et al., 2000). Early juveniles have been caught a few hundred meters above active vents along the ridge axis, suggesting that they actively migrate in the bathypelagic environment before recruitment (Herring & Dixon, 1998). They then return to vent sites as much larger juveniles than the larvae initially released into the water column (Methou et al., 2022). Whether larvae reach the photic zone of the ocean to feed on phytoplankton or feed at bathyal depths from sunken materials remains unknown. Vertical migration from hydrothermal vents to the surface has been suggested in the phenacolepadid limpet *Shinkailepas myojinensis* in the Western Pacific from in vivo larval experimentations (Yahagi et al., 2017) and was also demonstrated in the deep-sea seep mussel *Gigantidas childressi* (Arellano et al., 2014). Surface migration could, therefore, be the mechanism by which some vent species can achieve high dispersal along the ridge taking advantage of the stronger surface currents. Such mechanism was indeed suggested for the MAR vent gastropod *Divia briandi* (a phenacolepadid limpet like *S. myojinensis*) to explain its lack of genetic structure at the ridge scale, as determined by a mitochondrial gene (Yahagi et al., 2019). However, experimental work with the embryonic or larval stages of alvinocaridid shrimps suggests that the characteristics of these life stages may not be optimal to cope with the temperature and pressure of the photic ocean layer and that they may instead remain below the thermocline (Methou, Guéganton, et al., 2024; Tyler & Dixon, 2000).

The lack of genetic structure in vent shrimps contrasts sharply with recent population genomics studies that have been done on either the Atlantic vent mussels (Breusing et al., 2016; Van Der Heijden et al., 2012) or the vent gastropods *Lepetodrilus atlanticus* and *Peltospira smaragdina* (Portanier et al. in press), which all display highly structured populations along the Mid-Atlantic Ridge. Although the two gastropod genera have lecithotrophic larvae with likely deep-water dispersal (Chen et al., 2025; Mullineaux et al., 1996), *Bathymodiolus* vent mussels possess planktotrophic larvae with a relatively long pelagic larval duration. The difference between shrimps and mussels remains unclear, this could be due to the shrimp larvae being better at selecting the water layer to disperse in, or the result of

408 environmental factors limiting the mussels' dispersal, or the mussels having a shorter pelagic larval
409 duration than shrimps.

410 Vent shrimp populations studied here all appear to contribute migrants that could reach other
411 sites and participate in the renewal of other local populations, apparently without suffering regional
412 connectivity restrictions, as observed in other vent species (Gollner et al., 2016; Methou, Ogawa, et al.,
413 2024; Yahagi et al., 2019; Y. Zhou et al., 2022). Connectivity networks may however be affected by
414 the impacts of mining activities, which are not limited to the seafloor, but potentially far reaching in the
415 water column (Menini & Van Dover, 2019). Indeed, the persisting lack of knowledge on shrimp
416 planktonic larval stages regarding their location above the seafloor, their specific physiological
417 requirements, or their reliance on specific navigation cues to re-establish themselves at vents, make
418 predictions on the impacts of mining extractive activities on connectivity networks highly uncertain.

419 *4.2. Caribbean-Atlantic connectivity of the* Rimicaris chacei / R. hybisae *complex*

420 The MCSC constitutes a unique and isolated vent biogeographic province in the Atlantic. It has
421 one of the lowest faunal richness and comprises species that are unique to the region but also species
422 that are shared with methane seeps in the Gulf of Mexico (Georgieva et al., 2023; Linse et al., 2019;
423 Plouviez et al., 2015). Our results revealed a strong connection between the MCSC and the MAR vent
424 fauna: the dominant MCSC taxon, *R. hybisae*, shares a population history with the MAR *R. chacei*
425 shrimp population, exhibiting minimal genetic differentiation and contemporary gene flow. In addition,
426 the lack of a fixed divergence both at the mitochondrial (Methou, Guéganton, et al., 2024) and nuclear
427 (present study) genome scales further supports the hypothesis of a single species cross-exchanging
428 genes between the MAR and MCSC. Based on these results, it is now clear that *R. chacei* and *R. hybisae*
429 represent two distinct phenotypes or forms of a single species and we here synonymise them. *Rimicaris*
430 *chacei* is the earlier name and has precedence over *R. hybisae* (see: section 5. Systematics).

431 The demogenetic analysis conducted by DILS (Fraïsse et al., 2021) clearly indicated the
432 presence of a single shrimp population, with the *hybisae* and *chacei* forms exhibiting identical genetic
433 diversity and minimal population differentiation. This contrasted with the geographic variation detected

434 by the discriminating analysis of DAPC on the whole set of SNPs obtained from the shrimp genome.
435 As DILS employed subsamples of 1,000 loci at each step of the ABC analysis, some population
436 divergence was probably not detected – most likely because differentiated SNPs were rare – which
437 made it easy to reject the strict isolation model but difficult to select the appropriate isolation-with-
438 migration model. While genetic variables best fit the secondary contact model (SC_1m_2N), the
439 DILS_2populations analysis makes it difficult to choose between models of secondary contact (SC),
440 isolation with migration (IM) and ancient migration (AM) depending on the filtering parameters.
441 Nevertheless, all models with migration agree that the two shrimp ecotypes have been separated for
442 only a very short time, approximately less than 2,000 generations. This is much shorter than the
443 estimated divergence time between geographic populations of several vent species including
444 gastropods, mussels, polychaetes and barnacles, in back-arc basins of the southwestern Pacific (Tran
445 Lu Y et al., 2022), or between southern and northern populations of several species in the East Pacific
446 Rise (Matabos et al., 2011; Plouviez et al., 2009). It is therefore consistent with the hypotheses of
447 ongoing migration between the MCSC and MAR, and of a rapid expansion following their initial
448 separation, to explain the low genetic diversity observed despite large population sizes.

449 All isolation-with-migration models also indicated that populations of both *chacei* and *hybisae*
450 forms increased rapidly by at least one order of magnitude following the split of the ancestral
451 population. A possible explanation for this sudden and simultaneous population expansion could be the
452 recent and shared acquisition of a trophic chemosynthetic symbiosis, which has been ecologically
453 successful at several hydrothermal vent fields across the North Atlantic and Caribbean Sea (Methou et
454 al., 2020; Methou, Guéganton, et al., 2024). Furthermore, *R. chacei* populations are growing faster
455 possibly at the expense of *R. hybisae* populations, with reliable asymmetry in migration from the MCSC
456 to the MAR, regardless of the chosen model. Although *R. chacei* populations are currently far smaller
457 than those of their ecological challenger, *R. exoculata,* at MAR vents, this population increase is partly
458 validated by the discovery of dense aggregations of *R. chacei* juveniles in nurseries at the TAG and
459 Snake Pit vent fields despite a high post-settlement mortality (Hernández-Ávila et al., 2022; Methou et
460 al., 2022). However, even if there is currently a massive recruitment of *R. chacei* juveniles at MAR

vents, their genetic signatures are not different from those of adults and are not indicative of first- or second generation of migrants from MCSC. Consequently, the connection between the shrimp populations of the MCSC and MAR vents is probably indirect and should require intermediate active sites.

The bidirectionality of gene flow between the MAR and MCSC shrimp populations calls into question the lack of *R. exoculata* colonization at the MCSC vent fields. This can be viewed as either the migration of *R. chacei* forms being more asymmetrical than predicted by the model or, that *R. exoculata* is less able to migrate to the MCSC. Firstly, the co-occurring *Rimicaris* shrimps from the MAR exhibit different distributions and likely distinct demographic histories within the Atlantic Ocean, which may be related to the use of different dispersal routes. Despite sharing similar larval characteristics in the early stages (Hernández-Ávila et al., 2015), *R. exoculata* and *R. chacei* clearly differ in their juvenile sizes at settlement as well as in their isotopic niches that segregate in their carbon source in the earliest stages suggesting distinct larval histories (Methou et al., 2020). Secondly, co-occurring vent species often exhibit different connectivity patterns even between closely related species within the same genus due to specific combination of biological traits and habitat requirements (Chen et al., 2025; Methou et al., 2025; Poitrimol et al., 2022). In the case of the *Peltospira* species along the MAR, the restricted range of *P. gargantua* to the Hydra and Falkor EMARK vent fields, as opposed to the broader distribution of *P. smaragdina* across the northern MAR, has been attributed to specific environmental filters related to the geochemistry of these vents rather than to larval dispersal ability (Chen et al., 2025). Therefore, the two species likely have both different plastic responses to environmental variations and distinct larval life capabilities, resulting in different vertical distributions in the water column. This could prevent *R. exoculata* from reaching the Caribbean Sea during its dispersal phase.

4.3. Evolutionary implications of becoming a species with two distinct ecotypes

Contemporary exchanges of migrants between the MAR and MCSC shrimp populations suggests a strong ecological plasticity of the 'panmictic' species in terms of trophic behavior and habitat use. The *hybisae* form predominantly feeds on chemoautotrophic production, possibly from its

488 cephalothoracic symbionts. It lives in dense aggregates and shows an enlarged cephalothorax. The
489 *chacei* form shows limited anatomical changes during its metamorphosis with a less developed
490 cephalothorax. It has a mixed diet, partially uses chemoautotrophic bacterial production, and lives in
491 smaller groups (Methou et al., 2022; Methou, Guéganton, et al., 2024; Nye et al., 2013). It has been
492 suggested that individuals of *R. chacei* could have a limited "critical period" during their metamorphosis
493 that determines their developmental trajectory, whether an energetically viable symbiosis has been
494 established before or after this window of competency (Methou, Guéganton, et al., 2024). Among
495 factors that can affect their developmental trajectories, competition for space with *R. exoculata* on the
496 MAR for access to suitable vent fluid sources and symbionts during the juvenile stages may drive
497 development towards the *chacei* form. This is supported by the strong spatial segregation of the juvenile
498 stages of *R. exoculata* and *R. chacei*; the latter is confined to more distant nursery habitats (Hernández-
499 Ávila et al., 2022; Methou et al., 2022).

500 However, competition for a trophic niche should not entirely eliminate the *hybisae* form at
501 MAR vent sites. Indeed, even in the absence of their *R. exoculata* competitor, *R. chacei* shrimps from
502 the Lucky Strike vent field do not exhibit the inflated cephalothorax of the *hybisae* form. Thus, the
503 slight genetic differences between the *hybisae* and *chacei* forms depicted by the DAPC analysis could
504 be adaptive, regulating the molecular dialogue between the shrimp and its symbionts, and/or stabilising
505 the morphological change of *R. chacei* along the MAR. It is worth noting that none of the sequenced *R.*
506 *chacei* adults and juveniles had more than a 70% of '*hybisae'* ancestry.

507 Nevertheless, trophic plasticity also appears to be a common trait in *hybisae* populations on the
508 MCSC. Individuals found on the periphery exhibit mixotrophic behaviour similar to that observed in
509 *R. chacei*, feeding on the exoskeletons (moults) of their conspecifics (Versteegh et al., 2023). This
510 duality of feeding behaviour (symbiotrophy vs. carnivory or scavenging: (Methou et al., 2020) could
511 therefore be rooted in the plasticity and polymorphism of the species and, expressed differentially
512 depending on habitat conditions and access to resources. Other cases of plasticity in relation to their
513 habitat are already known in vent ecosystems, such as the "short-fat" or a "long-skinny" morphotypes
514 of *Ridgeia piscesae* (Tunnicliffe et al., 2014) or the substrate-dependent shell morphologies of

515 *Lepetodrilus nux* (Chen & Watanabe, 2020). Hence, some species possess distinct adult ecotypes able
516 to colonise different habitats thanks to a complex interplay of genetic, epigenetic, and environmental
517 determinants (Barrett & Schluter, 2008; Gore et al., 2018; Krishnan & Rohner, 2017; Schwander et al.,
518 2010). The recent expansion of *R. chacei* can have led to allele surfing in the MAR populations that is
519 known to promote rapid adaptation from the standing genetic variation (Barrett & Schluter, 2008;
520 Excoffier & Ray, 2008), and hence the subtle genetic differentiation observed between its geographic
521 populations. Our results highlight phenotypic and trophic plasticity as an important adaptive strategy to
522 survive and thrive in hydrothermal vents, one of the Earth's most dynamic ecosystems.

523

524 # 5. Systematics

525 **Family Alvinocarididae Christoffersen, 1986**

526 **Genus Rimicaris Williams & Rona, 1986**

527 **Type species:** *Rimicaris exoculata* Williams & Rona, 1986

528 ***Rimicaris chacei* (Williams & Rona, 1986)**

529 *Rimicaris hybisae* Nye *et al.,* 2012; **syn. nov.**

530 **Diagnosis**

531 Adapted from (Komai & Segonzac, 2008) and (Nye et al., 2012). Carapace with broadly triangular or
532 rounded antennal lobe; pterygostomial lobe broadly rounded, less produced. Scaphognathite of maxilla
533 and caridean lobe of first maxilliped bearing numerous plumose seta-like structure on dorsal and ventral
534 surface; exopodal flagellum on first maxilliped completely reduced. Appendix masculina tapering
535 distally with 4-5 (*chacei* form) or 7–8 (*hybisae* form) spiniform setae restricted to tip. Uropodal
536 protopod posterolateral projection triangular with acute tip.

537 Characters specific to the *chacei* form on the MAR: Rostrum bluntly triangular, overreaching anterior
538 margins of eye-talks or tips of antennal lobes by less than half of its length; ventral surface slightly

539 convex. Antennae suboperculate, directed downward; distolateral tooth subacute or blunt (Komai &
540 Segonzac, 2008).

541 Characters specific to the *hybisae* form on the MCSC: Anterolateral region of the carapace inflated.
542 Rostrum reduced to broadly rounded lobe, nearly reaching, reaching, or slightly overreaching anterior
543 margins of medially-fused eyes; ventral surface flat or slightly convex. Four-lobed dorsal organ; lobes
544 fused anteriorly; posterior lobes with paired "pores". Antennae not operculiform; distolateral tooth
545 subacute or blunt (Nye et al., 2012).

546 **Remarks**

547 We here synonymise *R. hybisae* Nye *et al*., 2012 with *R. chacei* (Williams & Rona, 1986).
548 *Rimicaris hybisae* was described as morphologically most similar to *R. exoculata*, *R. kairei* and *R.*
549 *chacei* because of the reduction of the rostrum, the presence of plumose-seta like structures on the dorsal
550 and ventral surfaces of enlarged mouthparts and an appendix masculina armed with distal setae only
551 (Nye et al., 2012). However, it can be distinguished from *R. exoculata* and *R. kairei* by the slightly less
552 inflated carapace and from *R. chacei* by the more inflated anterolateral region of the carapace, the
553 possession of a four-lobed dorsal organ, and of an acute tip on the uropodal protopod (Nye et al., 2012).
554 Recent work has shown that carapace inflation and the acquisition of a four-lobed dorsal organ are
555 morphological characteristics acquired during metamorphosis with a differentiation of developmental
556 trajectories between *R. chacei* and *R. hybisae* which only appears during this developmental phase with
557 indistinguishable morphologies between the two species at juvenile stages (Methou, Guéganton, et al.,
558 2024). Moreover, several morphological features of their internal anatomy, with equivalent stomach
559 size and mouthparts surface areas at adult stage, support the conspecificity of *R. chacei* and *R. hybisae*
560 (Guéganton, et al., 2024). Our work, using multiple single nucleotide positions (SNPs) markers support
561 the existence of a single genetic cluster for *R. hybisae* and *R. chacei*, already suggested by previous
562 work based on partial fragment of the mitochondrial COI gene (Teixeira et al., 2013; Vereshchaka et
563 al., 2015), and also on partial fragments of 16S, 18S, 28S and H3 genes (Methou, Guéganton, et al.,
564 2024).

Distribution and habitat

The typical form is known at several hydrothermal vents on the MAR including Lucky Strike, Rainbow, Broken Spur, TAG, Hydra, Snake Pit, Puy des Folles, Logatchev and Ashadze vent fields, at depths of 1700–4088 m (Cambon, 2023; Komai & Segonzac, 2008). The form *hybisae* is known from the Von Damm and Beebe vent fields on the MCSC at depths of 2300–4960 m (Nye et al., 2012). Adults are observed both in dense aggregations of thousands of individuals around vent chimneys and scattered at the periphery on the MCSC (Nye et al., 2013) but mostly observed as scattered individuals or in small aggregations between rocks or behind mussel beds on the MAR (Methou et al., 2022). Juveniles were also observed in dense aggregations close to low diffuse emissions on the MAR (Methou et al., 2022). A relatively dense aggregation of *R. chacei* was also recently observed at the TAG vent field in November 2023 (Figure S8; Bicose 3 expedition; https://doi.org/10.17600/18002399).

References

Adams, D. K., Arellano, S. M., & Govenar, B. (2012). Larval dispersal: Vent life in the water column. *Oceanography*, *25*(1), 256–268. https://doi.org/10.5670/oceanog.2012.24

Alexander, D. H., & Lange, K. (2011). Enhancements to the ADMIXTURE algorithm for individual ancestry estimation. *BMC Bioinformatics*, *12*(1). https://doi.org/10.1186/1471-2105-12-246

Andrews, S. (2010). FastQC: a quality control tool for high throughput sequence data. *Version 0.10*, *1*.

Arellano, S. M., Van Gaest, A. L., Johnson, S. B., Vrijenhoek, R. C., & Young, C. M. (2014). Larvae from deep-sea methane seeps disperse in surface waters. *Proceedings of the Royal Society B: Biological Sciences*, *281*(1786), 20133276. https://doi.org/10.1098/rspb.2013.3276

Barrett, R. D. H., & Schluter, D. (2008). Adaptation from standing genetic variation. *Trends in Ecology and Evolution*, *23*(1), 38–44. https://doi.org/10.1016/j.tree.2007.09.008

Beaulieu, S. E., Baker, E. T., & German, C. R. (2015). Where are the undiscovered hydrothermal vents on oceanic spreading ridges? *Deep Sea Research Part II: Topical Studies in Oceanography*, *121*, 202–212. https://doi.org/10.1016/j.dsr2.2015.05.001

Benjamini, Y., & Hochberg, Y. (1995). Controlling the False Discovery Rate: A Practical and Powerful Approach to Multiple Testing. *Journal of the Royal Statistical Society Series B: Statistical Methodology*, *57*(1), 289–300. https://doi.org/10.1111/j.2517-6161.1995.tb02031.x

Brelsford, A., Dufresnes, C., & Perrin, N. (2016). High-density sex-specific linkage maps of a European tree frog (Hyla arborea) identify the sex chromosome without information on offspring sex. *Heredity*, *116*(2), 177–181. https://doi.org/10.1038/hdy.2015.83

Breusing, C., Biastoch, A., Drews, A., Metaxas, A., Jollivet, D., Vrijenhoek, R. C., Bayer, T., Melzner, F., Sayavedra, L., Petersen, J. M., Dubilier, N., Schilhabel, M. B., Rosenstiel, P., & Reusch, T. B. H. (2016). Biophysical and Population Genetic Models Predict the Presence of "Phantom" Stepping Stones Connecting Mid-Atlantic Ridge Vent Ecosystems. *Current Biology*, *26*(17), 2257–2267. https://doi.org/10.1016/j.cub.2016.06.062

Breusing, C., Vrijenhoek, R. C., & Reusch, T. B. H. (2017). Widespread introgression in deep-sea hydrothermal vent mussels. *BMC Evolutionary Biology*, *17*(1), 1–10. https://doi.org/10.1186/s12862-016-0862-2

Cambon, M.-A. (2023). *Rapport de campagne BICOSE 3 2023*. https://campagnes.flotteoceanographique.fr/campagnes/18002399/fr/

Cambon-Bonavita, M.-A., Aubé, J., Cueff-Gauchard, V., & Reveillaud, J. (2021). Niche partitioning in the Rimicaris exoculata holobiont: The case of the first symbiotic Zetaproteobacteria. *Microbiome*, *9*(1), 1–16. https://doi.org/10.1186/s40168-021-01045-6

Catchen, J. M., Amores, A., Hohenlohe, P., Cresko, W., & Postlethwait, J. H. (2011). *Stacks*: Building and Genotyping Loci *De Novo* From Short-Read Sequences. *G3 Genes|Genomes|Genetics*, *1*(3), 171–182. https://doi.org/10.1534/g3.111.000240

Chang, C. C., Chow, C. C., Tellier, L. C., Vattikuti, S., Purcell, S. M., & Lee, J. J. (2015). Second-generation PLINK: Rising to the challenge of larger and richer datasets. *Gigascience*, *4*(1). https://doi.org/10.1186/s13742-015-0047-8

Chen, C., Pradillon, F., Diaz-Recio Lorenzo, C., & Alfaro-Lucas, J. M. (2025). Integrative taxonomy of two new peltospirid gastropods from Mid-Atlantic Ridge hot vents, including a potentially symbiotic species. *Zoological Journal of the Linnean Society*, *204*(2), zlaf055. https://doi.org/10.1093/zoolinnean/zlaf055

Chen, C., & Watanabe, H. K. (2020). Substrate-dependent shell morphology in a deep-sea vetigastropod limpet. *Marine Biodiversity*, *50*(6), 104. https://doi.org/10.1007/s12526-020-01135-y

Cuvelier, D., Matabos, M., & Sarrazin, J. (2025). Peltospira smaragdina gastropod assemblages as pioneers in Atlantic hydrothermal vent community succession. *Marine Biology*, *172*(9), 136. https://doi.org/10.1007/s00227-025-04695-4

Daguin Thiebaut, C., Ruault, S., Roby, C., Broquet, T., Viard, F., & Brelsford, A. (2021). *Construction of individual ddRAD libraries v1*. Springer Science and Business Media LLC. https://doi.org/10.17504/protocols.io.bv4tn8wn

Danecek, P., Auton, A., Abecasis, G., Albers, C. A., Banks, E., DePristo, M. A., Handsaker, R. E., Lunter, G., Marth, G. T., Sherry, S. T., McVean, G., Durbin, R., & 1000 Genomes Project

Analysis Group. (2011). The variant call format and VCFtools. *Bioinformatics*, *27*(15), 2156–2158. https://doi.org/10.1093/bioinformatics/btr330

Desbruyères, D., Almeida, A., Biscoito, M., Comtet, T., Khripounoff, A., Le Bris, N., Sarradin, P. M., & Segonzac, M. (2000). A review of the distribution of hydrothermal vent communities along the northern Mid-Atlantic Ridge: Dispersal vs. environmental controls. In M. B. Jones, J. M. N. Azevedo, A. I. Neto, A. C. Costa, & A. M. F. Martins (Eds.), *Island, Ocean and Deep-Sea Biology* (pp. 201–216). Springer Netherlands. https://doi.org/10.1007/978-94-017-1982-7_19

Diehl, A., & Bach, W. (2020). MARHYS (MARine HYdrothermal Solutions) Database: A Global Compilation of Marine Hydrothermal Vent Fluid, End Member, and Seawater Compositions. *Geochemistry, Geophysics, Geosystems*, *21*(12). https://doi.org/10.1029/2020gc009385

Faure, B., Jollivet, D., Tanguy, A., Bonhomme, F., & Bierne, N. (2009). Speciation in the deep sea: Multi-locus analysis of divergence and gene flow between two hybridizing species of hydrothermal vent mussels. *PLoS ONE*, *4*(8), 1–15. https://doi.org/10.1371/journal.pone.0006485

Fraïsse, C., Popovic, I., Mazoyer, C., Spataro, B., Delmotte, S., Romiguier, J., Loire, É., Simon, A., Galtier, N., Duret, L., Bierne, N., Vekemans, X., & Roux, C. (2021). DILS: Demographic inferences with linked selection by using ABC. *Molecular Ecology Resources*, *21*(8), 2629–2644. https://doi.org/10.1111/1755-0998.13323

Georgieva, M. N., Rimskaya-Korsakova, N. N., Krolenko, V. I., Van Dover, C. L., Amon, D. J., Copley, J. T., Plouviez, S., Ball, B., Wiklund, H., & Glover, A. G. (2023). A tale of two tubeworms: Taxonomy of vestimentiferans (Annelida: Siboglinidae) from the Mid-Cayman Spreading Centre. *Invertebrate Systematics*, *37*(3), 167–191. https://doi.org/10.1071/is22047

Gollner, S., Stuckas, H., Kihara, T. C., Laurent, S., Kodami, S., & Arbizu, P. M. (2016). Mitochondrial DNA Analyses Indicate High Diversity , Expansive Population Growth and High Genetic Connectivity of Vent Copepods (Dirivultidae) across Different Oceans. *PLoS ONE*, *11*(10), 1–23. https://doi.org/10.1371/journal.pone.0163776

Gore, A. V., Tomins, K. A., Iben, J., Ma, L., Castranova, D., Davis, A. E., Parkhurst, A., Jeffery, W. R., & Weinstein, B. M. (2018). An epigenetic mechanism for cavefish eye degeneration. *Nature Ecology and Evolution*, *2*(7), 1155–1160. https://doi.org/10.1038/s41559-018-0569-4

Guéganton, M., Methou, P., Aubé, J., Noël, C., Rouxel, O., Cueff, V., Gayet, N., Durand, L., Pradillon, F., & Cambon-Bonavita, A. (2024). Symbiont Acquisition Strategies in Post-Settlement Stages of Two Co-Occurring Deep-Sea Rimicaris Shrimp. *Ecology and Evolution*.

Hernández-Ávila, I., Cambon-Bonavita, M. A., & Pradillon, F. (2015). Morphology of first zoeal stage of four genera of alvinocaridid shrimps from hydrothermal vents and cold seeps: Implications for ecology, larval biology and phylogeny. *PLoS ONE*, *10*(12), 1–27. https://doi.org/10.1371/journal.pone.0144657

Hernández-Ávila, I., Cambon-Bonavita, M.-A., Sarrazin, J., & Pradillon, F. (2022). Population structure and reproduction of the alvinocaridid shrimp Rimicaris exoculata on the Mid-Atlantic Ridge: Variations between habitats and vent fields. *Deep Sea Research Part I: Oceanographic Research Papers*, *186*(June), 3–5. https://doi.org/10.1016/j.dsr.2022.103827

Herring, P. J., & Dixon, D. R. (1998). Extensive deep-sea dispersal of postlarval shrimp from a hydrothermal vent. *Deep-Sea Research Part I: Oceanographic Research Papers*, *45*(12), 2105–2118. https://doi.org/10.1016/S0967-0637(98)00050-8

Hurtado, L. A., Lutz, R. A., & Vrijenhoek, R. C. (2004). Distinct patterns of genetic differentiation among annelids of eastern Pacific hydrothermal vents. *Molecular Ecology*, *13*(9), 2603–2615. https://doi.org/10.1111/j.1365-294X.2004.02287.x

Jakobsson, M., & Rosenberg, N. A. (2007). CLUMPP: A cluster matching and permutation program for dealing with label switching and multimodality in analysis of population structure. *Bioinformatics*, *23*(14), 1801–1806. https://doi.org/10.1093/bioinformatics/btm233

Jombart, T. (2008). *adegenet*: A R package for the multivariate analysis of genetic markers. *Bioinformatics*, *24*(11), 1403–1405. https://doi.org/10.1093/bioinformatics/btn129

Jombart, T., & Ahmed, I. (2011). *adegenet 1.3-1*: New tools for the analysis of genome-wide SNP data. *Bioinformatics*, *27*(21), 3070–3071. https://doi.org/10.1093/bioinformatics/btr521

Komai, T., & Segonzac, M. (2008). Taxonomic Review of the Hydrothermal Vent Shrimp Genera Rimicaris Williams & Rona and Chorocaris Martin & Hessler (Crustacea: Decapoda: Caridea: Alvinocarididae). *Journal of Shellfish Research*, *27*(1), 21–41. https://doi.org/10.2983/0730-8000(2008)27%255B21:TROTHV%255D2.0.CO;2

Konn, C., Donval, J. P., Guyader, V., Germain, Y., Alix, A. S., Roussel, E., & Rouxel, O. (2022). Extending the dataset of fluid geochemistry of the Menez Gwen, Lucky Strike, Rainbow, TAG and Snake Pit hydrothermal vent fields: Investigation of temporal stability and organic contribution. *Deep-Sea Research Part I: Oceanographic Research Papers*, *179*(September 2021), 103630. https://doi.org/10.1016/j.dsr.2021.103630

Kopelman, N. M., Mayzel, J., Jakobsson, M., Rosenberg, N. A., & Mayrose, I. (2015). CLUMPAK: A program for identifying clustering modes and packaging population structure inferences across *K*. *Molecular Ecology Resources*, *15*(5), 1179–1191. https://doi.org/10.1111/1755-0998.12387

Krishnan, J., & Rohner, N. (2017). Cavefish and the basis for eye loss. *Philosophical Transactions of the Royal Society B: Biological Sciences*, *372*(1713). https://doi.org/10.1098/rstb.2015.0487

Linse, K., Nye, V., Copley, J. T., & Chen, C. (2019). On the systematics and ecology of two new species of Provanna (Gastropoda: Provannidae) from deep-sea hydrothermal vents in the Caribbean Sea and Southern Ocean. *Journal of Molluscan Studies*, *85*(4), 425–438. https://doi.org/10.1093/mollus/eyz024

Luu, K., Bazin, E., & Blum, M. G. B. (2017). *pcadapt*: An R package to perform genome scans for selection based on principal component analysis. *Molecular Ecology Resources*, *17*(1), 67–77. https://doi.org/10.1111/1755-0998.12592

Matabos, M., Cannat, M., Ballu, V., Barreyre, T., Blandin, J., Castillo, A., Cathalot, C., Chavagnac, V., Chu, N. C., Colaço, A., Crawford, W., Escartin, J., Ferron, B., Fontaine, F., Gautier, L., Godfroy, A., Laes-Huon, A., Lanteri, N., Leau, H., … Sarradin, P. M. (2025). The EMSO-Azores deep-sea observatory: 15 years of multidisciplinary studies of the lucky strike hydrothermal system, from sub-seafloor to the water column. *Journal of Sea Research*, *207*, 102625. https://doi.org/10.1016/j.seares.2025.102625

Matabos, M., Plouviez, S., Hourdez, S., Desbruyères, D., Legendre, P., Warén, A., Jollivet, D., & Thiébaut, E. (2011). Faunal changes and geographic crypticism indicate the occurrence of a biogeographic transition zone along the southern East Pacific Rise: Biogeographic transition zone along the southern EPR. *Journal of Biogeography*, *38*(3), 575–594. https://doi.org/10.1111/j.1365-2699.2010.02418.x

Menini, E., & Van Dover, C. L. (2019). An atlas of protected hydrothermal vents. *Marine Policy*, *108*, 103654. https://doi.org/10.1016/j.marpol.2019.103654

Methou, P., Guéganton, M., Copley, J. T., Kayama Watanabe, H., Pradillon, F., Cambon-Bonavita, M.-A., & Chen, C. (2024). Distinct development trajectories and symbiosis modes in vent shrimps. *Evolution*, *78*(3), 413–422. https://doi.org/10.1093/evolut/qpad217

Methou, P., Hernández-Ávila, I., Cathalot, C., Cambon-Bonavita, M.-A., & Pradillon, F. (2022). Population structure and environmental niches of Rimicaris shrimps from the Mid-Atlantic Ridge. *Marine Ecology Progress Series*, *684*, 1–20. https://doi.org/10.3354/meps13986

Methou, P., Johnson, S. B., Sherrin, J., Shank, T. M., Chen, C., & Tunnicliffe, V. (2025). A tale of two shrimps – Speciation and demography of two sympatric shrimp species from hydrothermal vents. *Molecular Ecology*, *34*(22). https://doi.org/10.1111/mec.70119

Methou, P., Michel, L. N., Segonzac, M., Cambon-Bonavita, M.-A., & Pradillon, F. (2020). Integrative taxonomy revisits the ontogeny and trophic niches of Rimicaris vent shrimps. *Royal Society Open Science*, *7*(7), 200837. https://doi.org/10.1098/rsos.200837

Methou, P., Ogawa, N. O., Nomaki, H., Ohkouchi, N., Chen, C., & Schnabel, K. (2024). Genetic connectivity and isotopic niches of alvinocaridid shrimps from chemosynthetic habitats in Aotearoa/New Zealand, with a new Alvinocaris species. *Marine Ecology Progress Series*. https://doi.org/10.3354/meps14611

Mullineaux, L. S., Kim, S. L., Pooley, A., & Lutz, R. A. (1996). Identification of archaeogastropod larvae from a hydrothermal vent community. *Marine Biology*, *124*, 551–560. https://doi.org/10.1007/BF00351036

Mullineaux, L. S., Metaxas, A., Beaulieu, S. E., Bright, M., Gollner, S., Grupe, B. M., Herrera, S., Kellner, J. B., Levin, L. A., Mitarai, S., Neubert, M. G., Thurnherr, A. M., Tunnicliffe, V.,

Watanabe, H. K., & Won, Y. J. (2018). Exploring the ecology of deep-sea hydrothermal vents in a metacommunity framework. *Frontiers in Marine Science*, *4*(FEB). https://doi.org/10.3389/fmars.2018.00049

Mullineaux, L. S., Mills, S. W., Le Bris, N., Beaulieu, S. E., Sievert, S. M., & Dykman, L. N. (2020). Prolonged recovery time after eruptive disturbance of a deep-sea hydrothermal vent community. *Proceedings of the Royal Society B: Biological Sciences*, *287*(1941), 20202070. https://doi.org/10.1098/rspb.2020.2070

Nye, V., Copley, J., & Plouviez, S. (2012). A new species of *Rimicaris* (Crustacea: Decapoda: Caridea: Alvinocarididae) from hydrothermal vent fields on the Mid-Cayman Spreading Centre, Caribbean. *Journal of the Marine Biological Association of the United Kingdom*, *92*(5), 1057–1072. https://doi.org/10.1017/S0025315411002001

Nye, V., Copley, J. T. P., & Tyler, P. A. (2013). Spatial Variation in the Population Structure and Reproductive Biology of Rimicaris hybisae (Caridea: Alvinocarididae) at Hydrothermal Vents on the Mid-Cayman Spreading Centre. *PLoS ONE*, *8*(3). https://doi.org/10.1371/journal.pone.0060319

O'Mullan, G. D., Maas, P. A. Y., Lutz, R. A., & Vrijenhoek, R. C. (2001). A hybrid zone between hydrothermal vent mussels (Bivalvia: Mytilidae) from the Mid-Atlantic Ridge. *Molecular Ecology*, *10*(12), 2819–2831. https://doi.org/10.1046/j.1365-294X.2001.t01-1-01401.x

Pembleton, L. W., Cogan, N. O. I., & Forster, J. W. (2013). St AMPP: An R package for calculation of genetic differentiation and structure of mixed-ploidy level populations. *Molecular Ecology Resources*, *13*(5), 946–952. https://doi.org/10.1111/1755-0998.12129

Plouviez, S., Jacobson, A., Wu, M., & Van Dover, C. L. (2015). Characterization of vent fauna at the mid-cayman spreading center. *Deep-Sea Research Part I: Oceanographic Research Papers*, *97*, 124–133. https://doi.org/10.1016/j.dsr.2014.11.011

Plouviez, S., Shank, T. M., Faure, B., Daguin-Thiebaut, C., Viard, F., Lallier, F. H., & Jollivet, D. (2009). Comparative phylogeography among hydrothermal vent species along the East Pacific Rise reveals vicariant processes and population expansion in the South. *Molecular Ecology*, *18*(18), 3903–3917. https://doi.org/10.1111/j.1365-294X.2009.04325.x

Poitrimol, C., Thiébaut, E., Daguin-Thiébaut, C., Le Port, A.-S., Ballenghien, M., Tran Lu Y, A., Hourdez, S., & Jollivet, D. (2022). Contrasted phylogeographic patterns of hydrothermal vent gastropods along South West Pacific: Woodlark Basin, a possible contact zone and/or stepping-stone. *PLoS ONE*, 1–27. https://doi.org/10.1371/journal.pone.0275638

Pond, D. W., Gebruk, A., Southward, E. C., Southward, A. J., Fallick, A. E., Bell, M. V., & Sargent, J. R. (2000). Unusual fatty acid composition of storage lipids in the bresilioid shrimp Rimicaris exoculata couples the photic zone with MAR hydrothermal vent sites. *Marine Ecology Progress Series*, *198*, 171–179. https://doi.org/10.3354/meps198171

Ponsard, J., Cambon-Bonavita, M.-A., Zbinden, M., Lepoint, G., Joassin, A., Corbari, L., Shillito, B., Durand, L., Cueff-Gauchard, V., & Compère, P. (2013). Inorganic carbon fixation by chemosynthetic ectosymbionts and nutritional transfers to the hydrothermal vent host-shrimp Rimicaris exoculata. *ISME Journal*, *7*(1), 96–109. https://doi.org/10.1038/ismej.2012.87

Privé, F., Luu, K., Vilhjálmsson, B. J., & Blum, M. G. B. (2020). Performing Highly Efficient Genome Scans for Local Adaptation with R Package pcadapt Version 4. *Molecular Biology and Evolution*, *37*(7), 2153–2154. https://doi.org/10.1093/molbev/msaa053

Purcell, S., Neale, B., Todd-Brown, K., Thomas, L., Ferreira, M. A. R., Bender, D., Maller, J., Sklar, P., De Bakker, P. I. W., Daly, M. J., & Sham, P. C. (2007). PLINK: A Tool Set for Whole-Genome Association and Population-Based Linkage Analyses. *The American Journal of Human Genetics*, *81*(3), 559–575. https://doi.org/10.1086/519795

Rochette, N. C., & Catchen, J. M. (2017). Deriving genotypes from RAD-seq short-read data using Stacks. *Nature Protocols*, *12*(12), 2640–2659. https://doi.org/10.1038/nprot.2017.123

Rochette, N. C., Rivera-Colón, A. G., & Catchen, J. M. (2019). Stacks 2: Analytical methods for paired-end sequencing improve RADseq-based population genomics. *Molecular Ecology*, *28*(21), 4737–4754. https://doi.org/10.1111/mec.15253

Roux, C., Fraïsse, C., Romiguier, J., Anciaux, Y., Galtier, N., & Bierne, N. (2016). Shedding Light on the Grey Zone of Speciation along a Continuum of Genomic Divergence. *PLOS Biology*, *14*(12), e2000234. https://doi.org/10.1371/journal.pbio.2000234

Sarrazin, J., Cathalot, C., Laes, A., Marticorena, J., Michel, L. N., & Matabos, M. (2022). Integrated Study of New Faunal Assemblages Dominated by Gastropods at Three Vent Fields Along the Mid-Atlantic Ridge: Diversity, Structure, Composition and Trophic Interactions. *Frontiers in Marine Science*, *9*, 925419. https://doi.org/10.3389/fmars.2022.925419

Sarrazin, J., Portail, M., Legrand, E., Cathalot, C., Laes, A., Lahaye, N., Sarradin, P. M., & Husson, B. (2020). Endogenous versus exogenous factors: What matters for vent mussel communities? *Deep Sea Research Part I: Oceanographic Research Papers*, *160*, 103260. https://doi.org/10.1016/j.dsr.2020.103260

Schwander, T., Lo, N., Beekman, M., Oldroyd, B. P., & Keller, L. (2010). Nature versus nurture in social insect caste differentiation. *Trends in Ecology and Evolution*, *25*(5), 275–282. https://doi.org/10.1016/j.tree.2009.12.001

Segonzac, M., de Saint Laurent, M., & Casanova, B. (1993). L'enigme du comportement trophique des crevettes Alvinocarididae des sites hydrothermaux de la dorsale medio-atlantique. *Cahiers de Biologie Marine*, *34*(4), 535–571. https://doi.org/10.21411/%2520CBM.A.B3683E29

Streit, K., Bennett, S. A., Van Dover, C. L., & Coleman, M. (2015). Sources of organic carbon for *Rimicaris hybisae*: Tracing individual fatty acids at two hydrothermal vent fields in the Mid-Cayman rise. *Deep Sea Research Part I: Oceanographic Research Papers*, *100*, 13–20. https://doi.org/10.1016/j.dsr.2015.02.003

Sundqvist, L., Keenan, K., Zackrisson, M., Prodöhl, P., & Kleinhans, D. (2016). Directional genetic differentiation and relative migration. *Ecology and Evolution*, *6*(11), 3461–3475. https://doi.org/10.1002/ece3.2096

Teixeira, S., Cambon-Bonavita, M. A., Serrão, E. A., Desbruyéres, D., & Arnaud-Haond, S. (2011). Recent population expansion and connectivity in the hydrothermal shrimp Rimicaris exoculata along the Mid-Atlantic Ridge. *Journal of Biogeography*, *38*(3), 564–574. https://doi.org/10.1111/j.1365-2699.2010.02408.x

Teixeira, S., Olu, K., Decker, C., Cunha, R. L., Fuchs, S., Hourdez, S., Serrão, E. A., & Arnaud-Haond, S. (2013). High connectivity across the fragmented chemosynthetic ecosystems of the deep

Atlantic Equatorial Belt: Efficient dispersal mechanisms or questionable endemism? *Molecular Ecology*, *22*(18), 4663–4680. https://doi.org/10.1111/mec.12419

Teixeira, S., Serrão, E. A., & Arnaud-Haond, S. (2012). Panmixia in a fragmented and unstable environment: The hydrothermal shrimp Rimicaris exoculata disperses extensively along the Mid-Atlantic ridge. *PLoS ONE*, *7*(6), 1–10. https://doi.org/10.1371/journal.pone.0038521

Thaler, A. D., Plouviez, S., Saleu, W., Alei, F., Jacobson, A., Boyle, E. A., Schultz, T. F., Carlsson, J., & Van Dover, C. L. (2014). Comparative population structure of two deep-sea hydrothermal-vent- associated decapods (Chorocaris sp. 2 and Munidopsis lauensis) from southwestern Pacific back-arc basins. *PLoS ONE*, *9*(7), 1–13. https://doi.org/10.1371/journal.pone.0101345

Tran Lu Y, A., Ruault, S., Daguin-Thiébaut, C., Castel, J., Bierne, N., Broquet, T., Wincker, P., Perdereau, A., Arnaud-Haond, S., Gagnaire, P.-A., Jollivet, D., Hourdez, S., & Bonhomme, F. (2022). Subtle limits to connectivity revealed by outlier loci within two divergent metapopulations of the deep-sea hydrothermal gastropod Ifremeria nautilei. *Molecular Ecology*, 1–46. https://doi.org/10.1111/mec.16430

Tunnicliffe, V., & Fowler, C. M. R. (1996). Influence of sea-floor spreading on the global hydrothermal vent fauna. *Letters to Nature*, *379*. https://doi.org/10.1038/379531a0

Tunnicliffe, V., St. Germain, C., & Hilário, A. (2014). Phenotypic Variation and Fitness in a Metapopulation of Tubeworms (Ridgeia piscesae Jones) at Hydrothermal Vents. *PLoS ONE*, *9*(10), e110578. https://doi.org/10.1371/journal.pone.0110578

Tyler, P. A., & Dixon, D. R. (2000). Temperature/pressure tolerance of the first larval stage of Mirocaris fortunata from Lucky Strike hydrothermal vent field. *Journal of the Marine Biological Association of the United Kingdom*, *80*(4), 739–740. https://doi.org/10.1017/S0025315400002605

Van Audenhaege, L., Sarrazin, J., Legendre, P., Perrois, G., Cannat, M., Arnaubec, A., & Matabos, M. (2024). Monitoring ecological dynamics on complex hydrothermal structures: A novel photogrammetry approach reveals fine-scale variability of vent assemblages. *Limnology and Oceanography*, *69*(2), 325–338. https://doi.org/10.1002/lno.12486

van der Heijden, K., Petersen, J. M., Dubilier, N., & Borowski, C. (2012). Genetic connectivity between north and south Mid-Atlantic Ridge chemosynthetic bivalves and their symbionts. *PLoS ONE*, *7*(7). https://doi.org/10.1371/journal.pone.0039994

Van Der Heijden, K., Petersen, J. M., Dubilier, N., & Borowski, C. (2012). Genetic Connectivity between North and South Mid-Atlantic Ridge Chemosynthetic Bivalves and Their Symbionts. *PLoS ONE*, *7*(7), e39994. https://doi.org/10.1371/journal.pone.0039994

Vereshchaka, A. L., Kulagin, D. N., & Lunina, A. A. (2015). Phylogeny and new classification of hydrothermal vent and seep shrimps of the family alvinocarididae (Decapoda). *PLoS ONE*, *10*(7), 1–29. https://doi.org/10.1371/journal.pone.0129975

Versteegh, E. A. A., Van Dover, C. L., Van Audenhaege, L., & Coleman, M. (2023). Multiple nutritional strategies of hydrothermal vent shrimp (*Rimicaris hybisae*) assemblages at the Mid-Cayman Rise. *Deep Sea Research Part I: Oceanographic Research Papers*, *192*, 103915. https://doi.org/10.1016/j.dsr.2022.103915

Weir, B. S., & Cockerham, C. C. (1984). Estimating F-Statistics for the Analysis of Population Structure. *Evolution*, *38*(6), 1358–1370. https://doi.org/10.2307/2408641

Yahagi, T., Fukumori, H., Warén, A., & Kano, Y. (2019). Population connectivity of hydrothermal-vent limpets along the northern Mid-Atlantic Ridge (Gastropoda: Neritimorpha: Phenacolepadidae). *Journal of the Marine Biological Association of the United Kingdom*, *99*(1), 179–185. https://doi.org/10.1017/S0025315417001898

Yahagi, T., Kayama Watanabe, H., Kojima, S., Kano, Y., Watanabe, H. K., Kojima, S., Kano, Y., Kayama Watanabe, H., Kojima, S., & Kano, Y. (2017). Do larvae from deep-sea hydrothermal vents disperse in surface waters? *Ecology*, *98*(6), 1524–1534. https://doi.org/10.1002/ecy.1800

Yahagi, T., Watanabe, H., Ishibashi, J. I., & Kojima, S. (2015). Genetic population structure of four hydrothermal vent shrimp species (Alvinocarididae) in the Okinawa Trough, Northwest Pacific. *Marine Ecology Progress Series*, *529*, 159–169. https://doi.org/10.3354/meps11267

Zbinden, M., & Cambon-Bonavita, M. (2020). Biology and ecology of Rimicaris exoculata, a symbiotic shrimp from deep-sea hydrothermal vents. *Marine Ecology Progress Series*, *652*, 187–222. https://doi.org/10.3354/meps13467

Zhou, H., Alexander, D., & Lange, K. (2011). A quasi-Newton acceleration for high-dimensional optimization algorithms. *Statistics and Computing*, *21*(2), 261–273. https://doi.org/10.1007/s11222-009-9166-3

Zhou, Y., Chen, C., Zhang, D., Wang, Y., Kayama, H., Jin, W., Dass, S., Ruiyan, B., Han, Y., Sun, D., Xu, P., Lu, B., Zhai, H., Han, X., Tao, C., Qiu, Z., Sun, Y., Liu, Z., Qiu, W., & Wang, C. (2022). Delineating biogeographic regions in Indian Ocean deep-sea vents and implications for conservation. *Diversity and Distributions*, *April*, 1–13. https://doi.org/10.1111/ddi.13535

Supporting Information

Additional supporting information may be found in the online version of the article at the publisher's website.

Conflict of Interest

Authors declare no conflict of interest.

Data Availability

The ddRAD sequences generated in this study are available from the European Nucleotide Archive database (project PRJEB61450).

Acknowledgment

We thank the captain, crew, and scientists on-board R/V *Pourquoi Pas?* during research expeditions SERPENTINE (https://doi.org/10.17600/7030030), MOMARDREAM (https://doi.org/10.17600/7030060), HERMINE (https://doi.org/10.17600/17000200) and BICOSE2 (https://doi.org/10.17600/18000004), on-board R/V *Atalante* during expeditions TRANSECT (https://doi.org/10.17600/18000513), MOMARSAT20 (https://doi.org/10.17600/18000684), and MOMARSAT21 (https://doi.org/10.17600/18001296), on-board R/V *Yokosuka* during expeditions YK13-05, and on-board R/V *James Cook* during expedition JC82. We extend the same to the pilots and technical teams of ROVs *Victor 6000* and *Isis* as well as the HOVs *Nautile* and *Shinkai 6500* during those expeditions. We gratefully acknowledge the cruise PIs for leading the expeditions:); Yves Fouquet, Ifremer (SERPENTINE & HERMINE); Françoise Gaill, Sorbonne Universités and Javier Escartin, ENS (MOMARDREAM); Cécile Cathalot and Ewan Pelleter, Ifremer (HERMINE); Marie-Anne Cambon, Ifremer (BICOSE2); Nadine Le Bris, Sorbonne Universités (TRANSECT); Pierre-Marie Sarradin and Julien Legrand, Ifremer (MOMARSAT20); Marjolaine Matabos and Jozée Sarrazin, Ifremer (MOMARSAT21); Ken Takai, JAMSTEC (YK13-05) and Jon Copley, NOC (JC82). Permission for sampling R. hybisae specimens in territorial waters of the Cayman Islands was issued by the appropriate UK authorities to R/V Yokosuka during YK13-05. We thank Dr. Jon Copley

(University of Southampton, UK) for providing *R. hybisae* samples from Von Damm collected during the JC82 expedition for our study, as well as Dr. Adrian Glover for the picture of *R. hybisae* (Figure 1C) took on board of the same expedition. This work benefited from access to the EMBRC-France and Biogenouest Genomer platform at the Station Biologique de Roscoff for ddRAD library size selection and quality control. We are also grateful to the Roscoff Bioinformatics platform ABiMS for access to the cluster for analyses and data storage. This project/work contributes the EMSO-Azores (https://www.emso-fr.org) regional node of the EMSO ERIC Research Infrastructure (https://emso.eu/) and was supported by the French Oceanographic Fleet (FOF https://www.flotteoceanographique.fr/en).

Fundings

EP and this work were supported by Ifremer through the project "Pourquoi Pas les Abysses" and fundings by the European Union's Horizon 2020 research and innovation program under grant agreement No 818123 (iAtlantic, https://www.iatlantic.eu/) and by France Génomique (ANR-10-INBS-09) and Genoscope-CEA through the project eDNAbyss (AP2016–228). PM was supported by ISblue project, Interdisciplinary graduate school for the blue planet (ANR-17-EURE-0015) and co-funded by a grant from the French government under the programme 'Investissements d'Avenir' embedded in France 2030: ANR-22-POCE-0007 (LIFEDEEPER).

935 **Figure Legend**

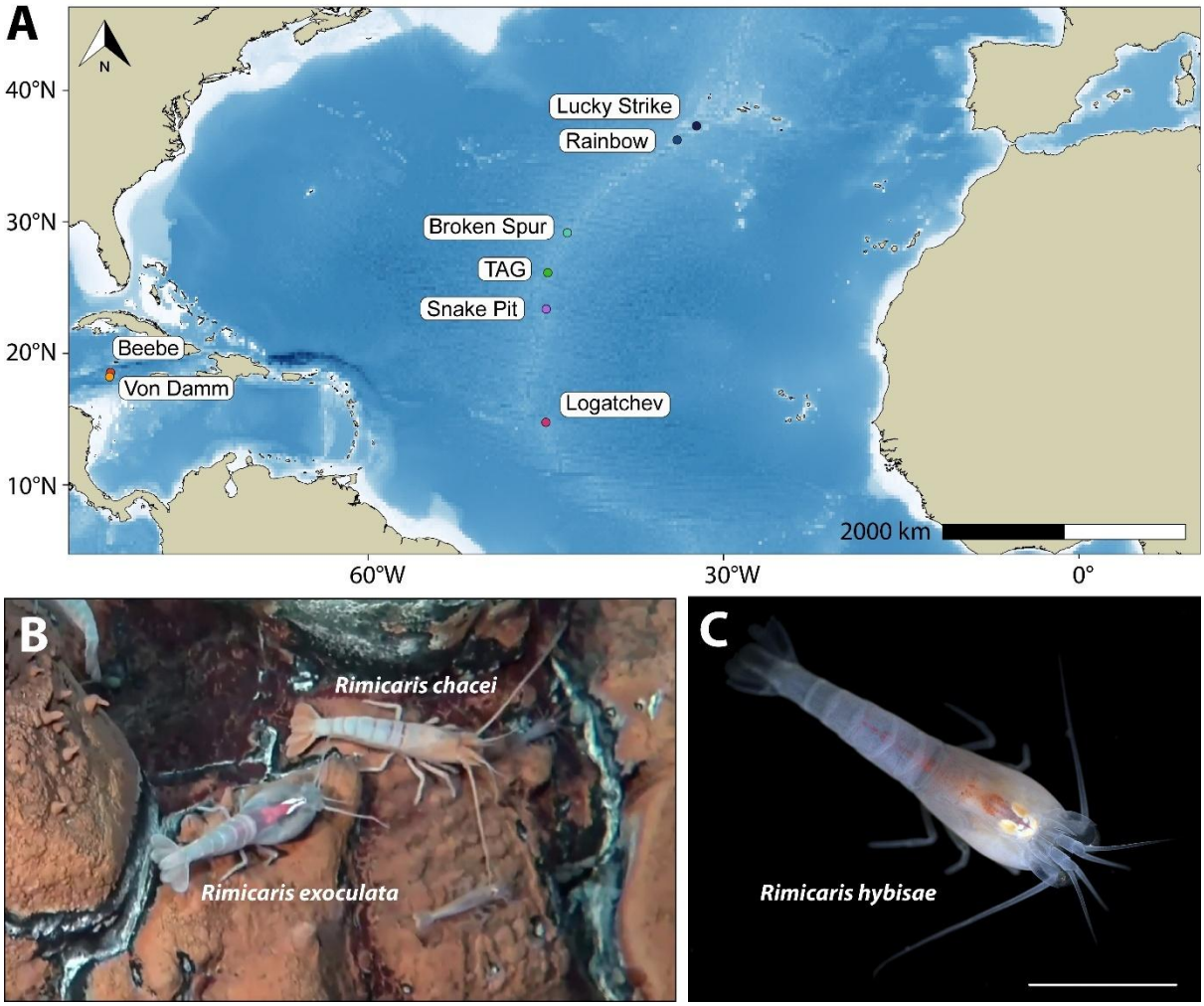

936

937 **Figure 1:** Context of the study. **A.** Map of hydrothermal vent fields sampled in the northern Atlantic
938 and the Caribbean Sea. Same color code for the different vent fields is applied for our genetic analyses
939 **B.** Two individuals of *R. exoculata* (right below) and *R. chacei* (left on top) on a rock close to
940 shimmering fluids at the TAG vent field (Credit: BICOSE 2 expedition; Ifremer). **C.** *R. hybisae*
941 individual from the Von Damm vent field (scale bar = 1mm) (Credit: Dr. Adrian Glover, Natural History
942 Museum UK).

943

944

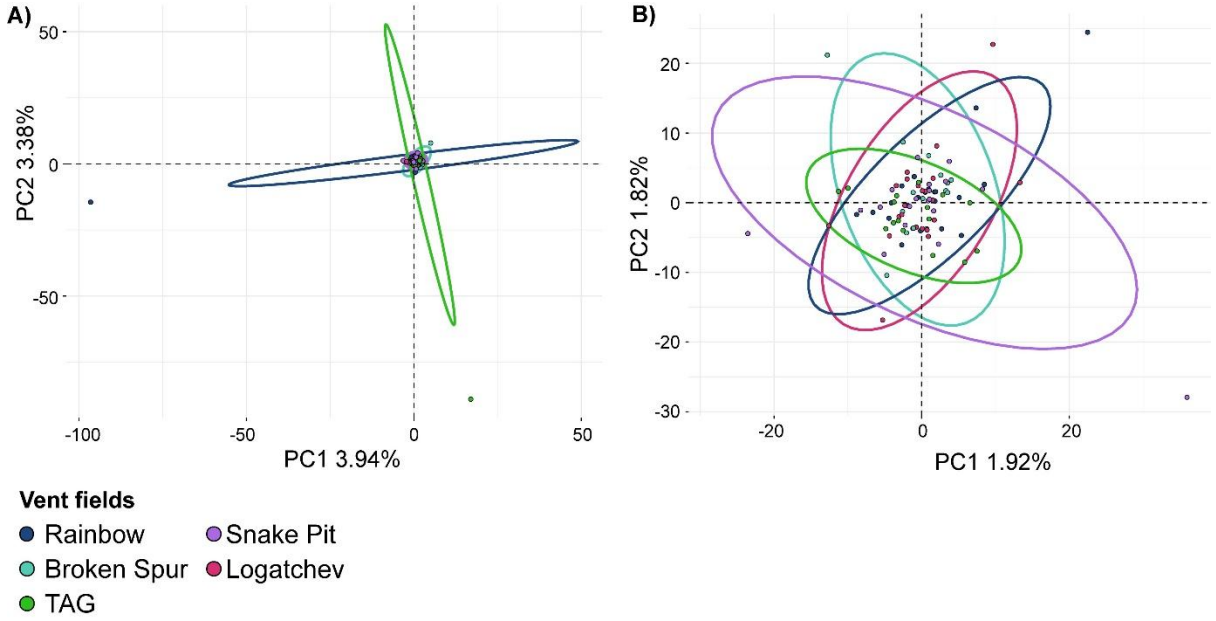

Figure 2: Population genetic structure of *Rimicaris exoculata* along the northern Mid-Atlantic Ridge **A.** Principal component analysis plot of genetic clusters considering all individuals **B.** or excluding 2 individuals that appear as outliers.

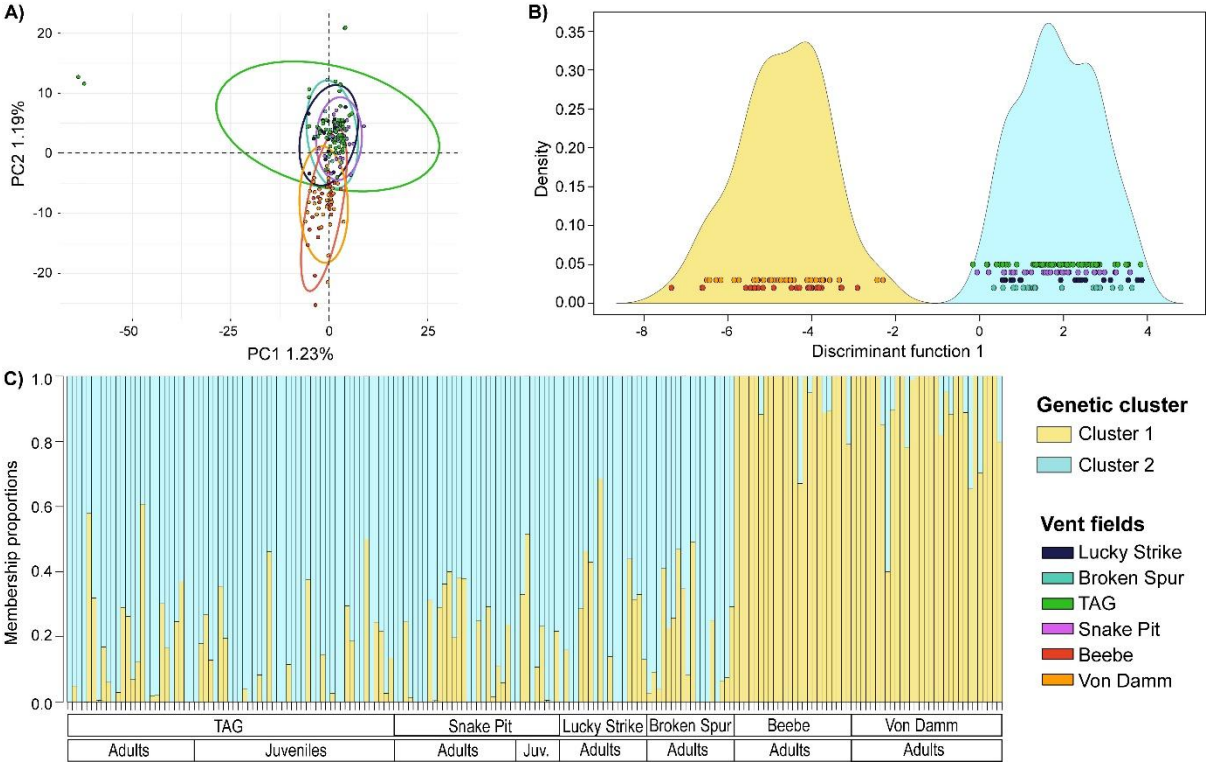

Figure 3: Population genetic structure of the *R. chacei* (Mid-Atlantic Ridge) and *R. hybisae* (Mid Cayman Spreading Center) complex of species. **A.** Principal component analysis plot of genetic clusters **B.** Discriminant Analysis of Principal Components (DAPC) genetic clusters **C.** ADMIXTURE membership proportions for *R. chacei/R. hybisae* complex of species.

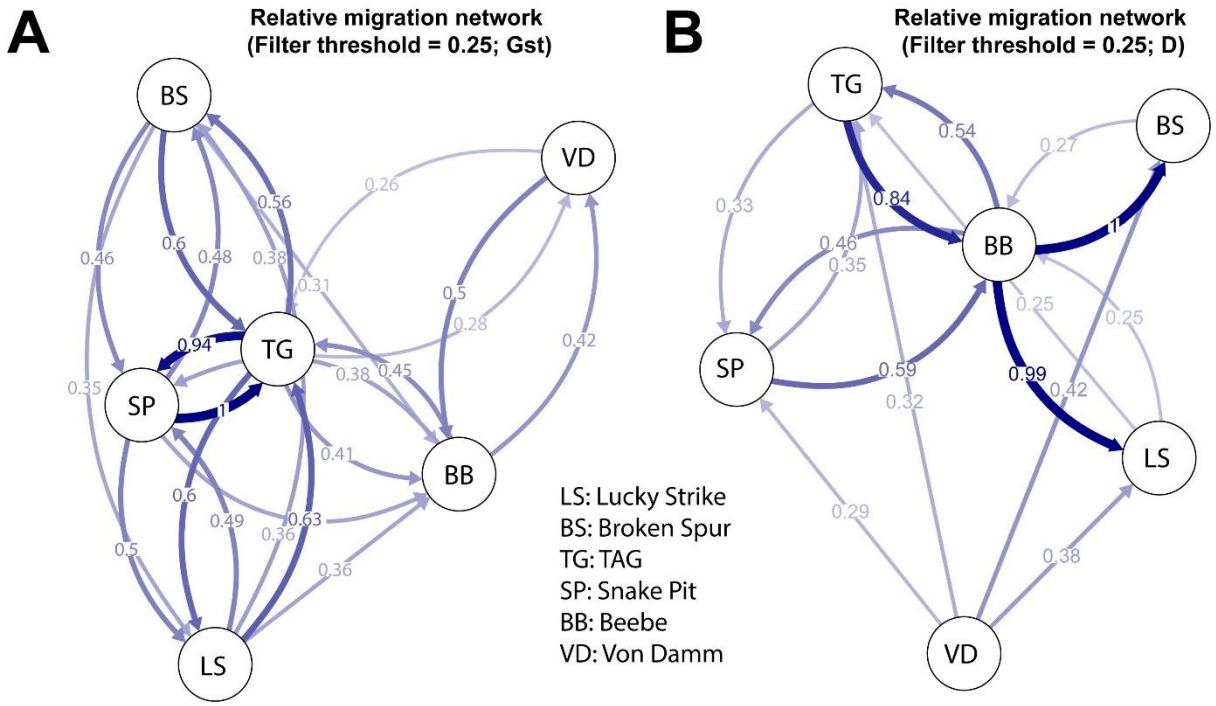

Figure 4. Relative migration networks of *R. chacei/hybisae* populations using divMigrate and based on **A.** Gst and **B.** Jost's D statistics. Each node represents a population from a given vent field.

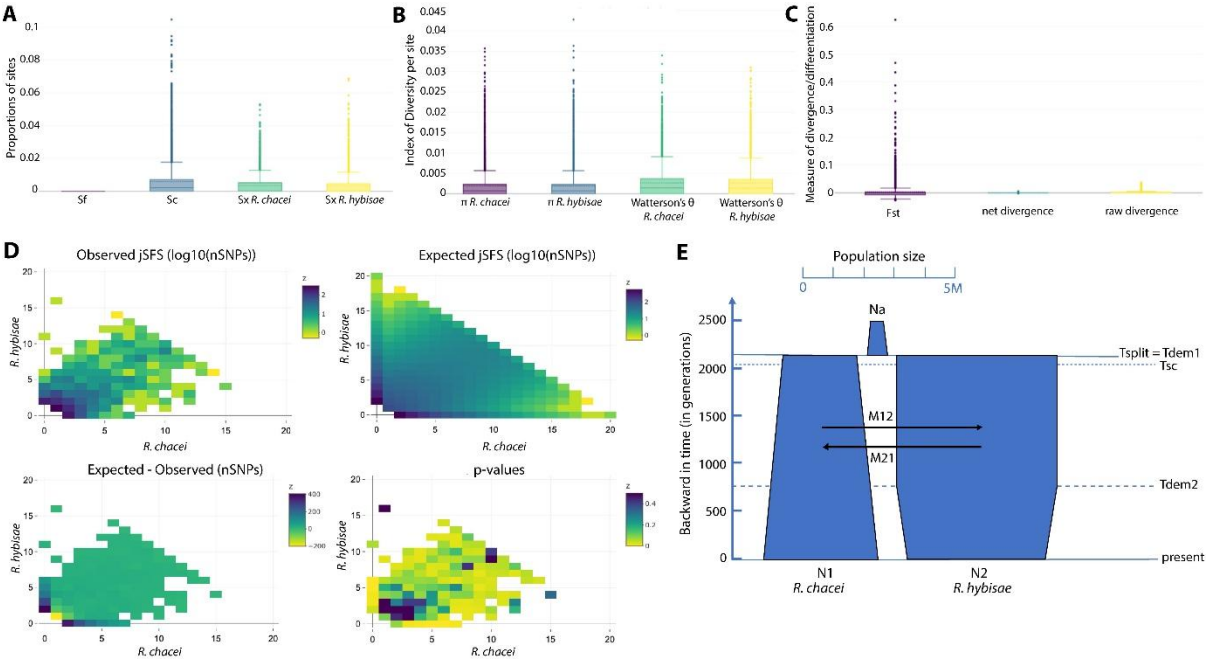

Figure 5. DILS analysis of the R. chacei/R. hybisae complex of species. **A.** Statistics displaying the number of bi-allelic sites shared (Ss) and fixed (Sf) between populations and the number of bi-allelic polymorphic sites (Sx) within each species. **B.** Nucleotide diversities (π or θ) **C.** Fst statistics **D.** Heatmap of both observed and expected 20x20 alleles joint site-frequency spectrum (jSFS) of the two shrimp populations (*R. chacei* vs *R. hybisae*) with residues and p-values of the model fit. **E.** Schematic graph of the evolution of the two ecotypes populations since their initial split following a SC_1m_2N model derived from the 2_populations DILS analysis. N_a= Ancestral population size, N_1 and N_2: sister population sizes, T_{split}= Time since population splitting, T_{dem1} and T_{dem2}: Times since population expansion or contraction, T_{sc}= Time since secondary contact, and M_{12} and M_{21}: numbers of migrants exchanged per generation between populations 1 and 2 in forward time.

979 # Tables

980 **Table 1:** Numbers of individuals of each species per vent field for which ddRAD data were obtained.

Vent field	***R. chacei***	***R. exoculata***	***R. hybisae***	**Total**
Lucky Strike	18			**18**
Rainbow		24		**24**
Broken Spur	18	16		**34**
TAG	67	18		**85**
Snake Pit	34	20		**54**
Logatchev		22		**22**
Beebe			24	**24**
Von Damm			31	**31**
Total	**137**	**100**	**55**	**292**

981

982

983 **Table 2:** Pairwise Fst values (below the diagonal with mean values and range under bracket) and Bonferroni corrected associated p-values (above

984 the diagonal) between vent fields sampled for *R. exoculata* and *R. chacei / R. hybisae* assemblies. Significantly different from zero values are bold.

R. exoculata					
	Rainbow	Broken Spur	Logatchev	TAG	Snake Pit
Rainbow	-	1.00	1.00	0.09	1.00
Broken Spur	0.0005 [-0.0026-0.0035]	-	1.00	0.27	0.62
Logatchev	-0.002 [-0.0042-0.0005]	-0.0013 [-0.0046-0.0021]	-	1.00	1.00
TAG	0.0043 [0.0006-0.0079]	0.0044 [-0.0001-0.0087]	0.0023 [-0.0013-0.0059]	-	**0.00**
Snake Pit	0.0005 [-0.0026-0.0037]	0.0030 [-0.0006-0.0066]	-0.0001 [-0.0028-0.0028]	**0.0061 [0.0017-0.0107]**	-

R. chacei / R. hybisae						
	BrokenSpur	Lucky Strike	Snake Pit	TAG	BeeBe	Von Damm
BrokenSpur	-	1.00	0.15	0.08	**0.00**	**0.00**
Lucky Strike	0.0003 [-0.0027-0.0033]	-	1.00	1.00	**0.00**	**0.00**
Snake Pit	0.0026 [0.0004-0.0049]	0.0007 [-0.002-0.0035]	-	0.23	**0.00**	**0.00**
TAG	0.0029 [0.0006-0.0051]	0.0016 [-0.0006-0.004]	0.0015 [0.0002-0.003]	-	**0.00**	**0.00**
BeeBe	**0.0234 [0.0126-0.037]**	**0.0223 [0.0127-0.0353]**	**0.0231 [0.0133-0.0356]**	**0.0233 [0.0145-0.0351]**	-	1.00
Von Damm	**0.0246 [0.0144-0.0371]**	**0.0218 [0.0126-0.0336]**	**0.0243 [0.0148-0.0358]**	**0.0233 [0.0147-0.0336]**	-0.0005 [-0.0021-0.0013]	-

985
986
987
988
989
990
991
992

993